International Journal of Nanomedicine

Dovepress
open access to scientific and medical research

Open Access Full Text Article

ORIGINAL RESEARCH

Multifunctional nanocomposite based on halloysite nanotubes for efficient luminescent bioimaging and magnetic resonance imaging

This article was published in the following Dove Press journal:
International Journal of Nanomedicine
19 September 2016
Number of times this article has been viewed

Tao Zhou[1]
Lei Jia[1]
Yi-Feng Luo[2]
Jun Xu[1]
Ru-Hua Chen[2]
Zhi-Jun Ge[2]
Tie-Liang Ma[2]
Hong Chen[2]
Tao-Feng Zhu[2]

[1]Department of Physics and Chemistry, Henan Polytechnic University, Jiaozuo, Henan, [2]The Affiliated Yixing Hospital of Jiangsu University, Yixing, Jiangsu, People's Republic of China

Abstract: A novel multifunctional halloysite nanotube (HNT)-based Fe_3O_4@HNT-polyethyleneimine-Tip-Eu(dibenzoylmethane)$_3$ nanocomposite (Fe-HNT-Eu NC) with both photoluminescent and magnetic properties was fabricated by a simple one-step hydrothermal process combined with the coupling grafting method, which exhibited high suspension stability and excellent photophysical behavior. The as-prepared multifunctional Fe-HNT-Eu NC was characterized using various techniques. The results of cell viability assay, cell morphological observation, and in vivo toxicity assay indicated that the NC exhibited excellent biocompatibility over the studied concentration range, suggesting that the obtained Fe-HNT-Eu NC was a suitable material for bioimaging and biological applications in human hepatic adenocarcinoma cells. Furthermore, the biocompatible Fe-HNT-Eu NC displayed superparamagnetic behavior with high saturation magnetization and also functioned as a magnetic resonance imaging (MRI) contrast agent in vitro and in vivo. The results of the MRI tests indicated that the Fe-HNT-Eu NC can significantly decrease the T_2 signal intensity values of the normal liver tissue and thus make the boundary between the normal liver and transplanted cancer more distinct, thus effectively improving the diagnosis effect of cancers.

Keywords: halloysite nanotube, lanthanide complex, iron oxide, luminescence, contrast agent

Introduction

Multifunctional luminescent and magnetic nanomaterials have been widely used in biomedical applications such as magnetic resonance imaging (MRI), bioimaging, targeted drug delivery, magnetic hyperthermia, and cell labeling and separation.[1–3] In recent years, organic dyes and quantum dots have been employed as biomedical fluorescent labels. However, these traditional fluorescent labels have limited use in large-scale applications due to their short lifetimes, photobleaching, and potential toxicity to cells.[4,5] To address the limitations of organic dyes and quantum dots, lanthanide complexes have been investigated as luminescent probes because of their excellent optical properties, including sharp emission bands, high quantum yields, long lifetime, high color purity, and large Stokes shift.[6,7] Unfortunately, the application of lanthanide complexes in biological imaging is limited by their low photochemical stability, hydrophobicity, and potential toxicity.[8] To solve these issues, luminescent nanocomposites (NCs) have been designed by incorporating lanthanide complexes into matrices, thus generating suitable diagnostic bioimaging probes with the intrinsic stability of inorganic matrices and the luminescent features of trivalent lanthanide ions.[9–11] In recent years, nanoclays have attracted considerable interest as supports due to their low cost, small size, and unusual chemically active surfaces.[12,13]

Correspondence: Lei Jia
Department of Physics and Chemistry, Henan Polytechnic University, No 2001, Shiji Street, Jiaozuo 454000, Henan, People's Republic of China
Tel/fax +86 391 398 7811
Email jlxj@hpu.edu.cn

Taofeng Zhu
The Affiliated Yixing Hospital of Jiangsu University, No 75, Tongzhenguan Road, Yixing 214200, Jiangsu, People's Republic of China
Tel +86 510 8792 1196
Fax +86 510 8792 1110
Email staff1639@yxph.com

submit your manuscript | www.dovepress.com
Dovepress
http://dx.doi.org/10.2147/IJN.S110081

Halloysite nanotube (HNT) is a two-layered aluminosilicate clay mineral with a chemical formula of $Al_2Si_2O_5(OH)_4 \cdot nH_2O$. It is a naturally occurring clay with a unique tubular nanostructure that has similar geometries to carbon nanotubes. Natural HNT clay has extremely high chemical stability, high surface area, and good adsorption properties. Because it is also environmentally friendly and biocompatible, it is suitable for biotechnological research.[14–16] In contrast to other nanoscale synthetic supports, it is inexpensive and readily obtainable in the People's Republic of China. These factors make HNT clay an optimal candidate for a support material. We have recently fabricated a visible-light-induced clay-based lanthanide polymer NC[17] that has potential applications in cell imaging due to its excellent luminescence, high suspension stability, and low cytotoxicity.

MRI is an effective clinical tool used for the diagnosis of many diseases. It offers several advantages, including high accuracy, rapid scanning, and a long effective imaging window. It provides a wealth of physiological and anatomical information on healthy or diseased internal organs and tissues.[18,19] Superparamagnetic iron oxide nanoparticles (NPs), such as Fe_3O_4 NPs, are strong enhancers of proton relaxation with superior magnetic resonance (MR) T_2 (transverse relaxation) shortening effects and can be used at a much lower concentration than paramagnetic agents.[20,21] When synthesizing multifunctional magnetic and luminescent nanomaterials, we found that the luminescence intensity of luminescent labels dropped when coupled directly to Fe_3O_4 NPs.[22] To avoid this quenching problem, we assembled Fe_3O_4@HNTs and functionalized the Fe_3O_4@halloysite with hydrophilic branched polyethyleneimine (PEI). We describe the applications of this multifunctional natural clay-based nanomaterial in bioimaging and MRI. To the best of our knowledge, this is the first example of magnetic natural clay-based lanthanide Fe_3O_4@HNT-PEI-Tip-Eu(dibenzoylmethane [DBM])$_3$ NC (Fe-HNT-Eu NC) suitable for MRI and luminescent bioimaging; the fabrication route is shown in Figure 1. This low-cost preparation produced an NC material possessing high suspension stability, low cytotoxicity, efficient luminescent emission, long luminescence lifetime, high quantum yield, and improved photoluminescence stability. Meanwhile, the NC could function as an MRI contrast agent in vitro and in vivo. These attributes highlight the potential of the as-prepared NC for luminescent bioimaging and MRI.

Materials and methods

Materials

5-Bromothiophene-2-carbaldehyde and 1,10-phenanthroline-5,6-dione were purchased from Acros Organics. 3-Iodopropyltrimethoxysilane (99%) and halloysite were purchased from Sigma-Aldrich Co. (St Louis, MO, USA). DBM, analytic reagent, and branched PEI with a molecular mass of 25 kDa were purchased from Aladdin Industrial Corporation. Europium chloride ($EuCl_3 \cdot 6H_2O$) was obtained by dissolving Eu_2O_3 (99.99%; Shanghai Yuelong) in hydrochloric acid,

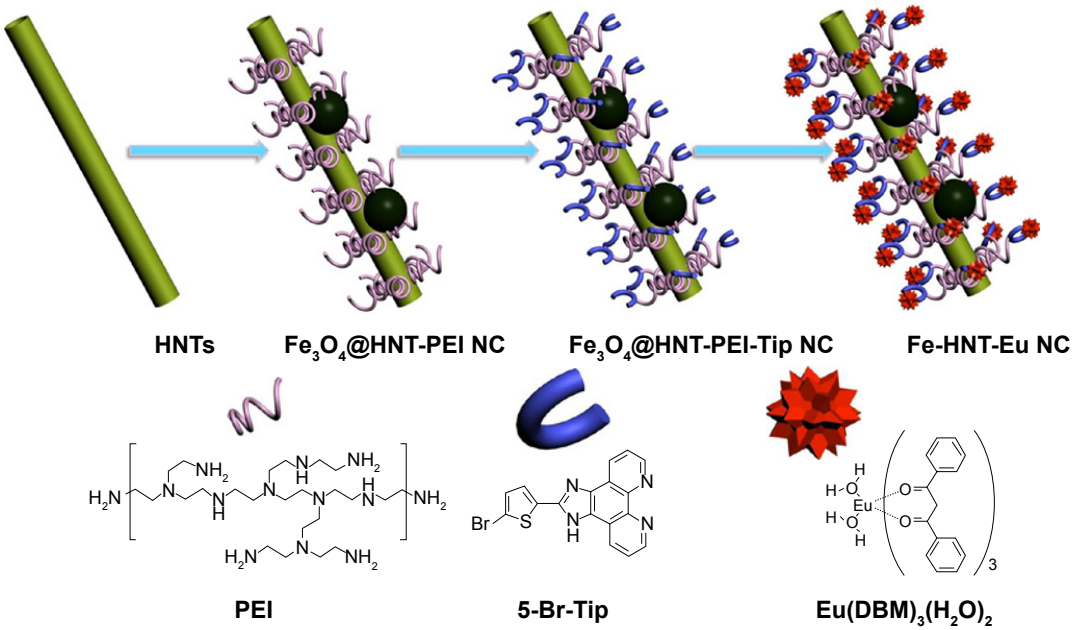

Figure 1 Schematic illustration of the synthesis of Fe-HNT-Eu NC.
Abbreviations: 5-Br-Tip, 2-(5-bromothiophen-2-yl)imidazo[4,5-f] [1,10]phenanthroline; DBM, dibenzoylmethane; HNT, halloysite nanotube; NC, nanocomposite; PEI, polyethyleneimine.

followed by successive fuming to remove excess acid. All other reagents were analytically pure and were purchased from the China National Medicines Group.

Dulbecco's Modified Eagle's Medium (DMEM) and fetal bovine serum were purchased from Thermo Fisher Scientific (Waltham, MA, USA). The fluorescein Annexin V-FITC and propidium iodide (PI) double staining kit was purchased from BD Biosciences (San Jose, CA, USA). Cell Counting Kit-8 (CCK8) assay kits were purchased from Kaiji BioTech (Nanjing, People's Republic of China). VX2 liver tumor-bearing rabbits were purchased from the Second People's Hospital of Lianyungang.

Synthesis

Amino modification of superparamagnetic Fe-HNT-Eu NC

A three-step modification procedure was used to fabricate superparamagnetic Fe_3O_4@HNT-PEI NC.[23] First, 1 g of $FeCl_3 \cdot 6H_2O$ was dissolved in 30 mL of ethylene glycol to form a clear solution. Then, 2.7 g of sodium acetate and 0.75 g of polyethylene glycol were added with constant stirring for 30 minutes. HNTs (300 mg) were then ultrasonically dispersed in the resulting dispersion for 3 hours. The mixture was sealed in a Teflon-lined stainless steel autoclave (50 mL capacity) and maintained at 200°C for 8 hours. The resulting functionalized NPs, denoted as Fe_3O_4@HNT, were then cooled to ambient temperature. The black magnetite particles were washed sequentially with ethanol and deionized water and dried under vacuum at 60°C for 24 hours. In the second step, Fe_3O_4@HNT NPs (300 mg) were dispersed in dry toluene (50 mL) using an ultrasonic bath. 3-Iodopropyltrimethoxysilane (0.5 mL) was added to the Fe_3O_4@HNT suspension, and the reaction mixture was heated to 110°C with mechanical stirring. After 8 hours, the solids were recovered using an NdFeB magnet, washed with ethanol three times to remove residual toluene and silane, and dried under vacuum. These NPs were denoted as Fe_3O_4@HNT-I. Finally, in the third step, Fe_3O_4@HNT-I NPs (300 mg) were suspended in *N*,*N*-dimethylformamide (DMF, 50 mL) with sonication. PEI (1.0 mL of a 50% aqueous solution) was added to the reaction mixture and heated to 130°C with mechanical stirring for 12 hours. The NPs were recovered using an NdFeB magnet, washed with ethanol three times to remove residual PEI, and dried under vacuum. These NPs were denoted as Fe_3O_4@HNT-PEI.

Synthesis of Fe_3O_4@HNT-PEI-Tip NC

The ligand 2-(5-bromothiophen-2-yl)imidazo[4,5-f] [1,10] phenanthroline (5-Br-Tip) was synthesized according to methods reported in the literature.[24] A mixture of 5-bromothiophene-2-carbaldehyde (0.230 g, 1.2 mmol), $AcONH_4$ (1.540 g, 1 mmol), and 1,10-phenanthroline-5,6-dione (0.21 g, 1 mmol) in AcOH (20 mL) was stirred and heated at 85°C for 4 hours. The mixture was then cooled to room temperature, and the product was precipitated during neutralization with 5 M NH_4OH. The precipitate was filtered, washed with H_2O and ethanol, recrystallized from MeOH, and dried under vacuum to yield a pure, light yellow product. Fe_3O_4@HNT-PEI (300 mg) and K_2CO_3 (138 mg, 1.0 mmol) were suspended in 30 mL of DMF, sonicated for 30 minutes, and then added to 20 mL of DMF containing the obtained 5-Br-Tip (381 mg, 1.0 mmol). The mixture was refluxed for 24 hours and centrifuged. After washing the resulting solids with DMF and ethanol (95%) and drying at 60°C, the NC Fe_3O_4@HNT-PEI-Tip was obtained.

Synthesis of Fe_3O_4@HNTs-PEI-Tip-Eu(DBM)$_3$

The complex $Eu(DBM)_3(H_2O)_2$ (43.0 mg, 0.05 mmol, prepared from DBM and $EuCl_3 \cdot 6H_2O$ according to the literature[25]) was refluxed with 300 mg of Fe_3O_4@HNT-PEI-Tip in ethanol. The suspension was collected by centrifugation after 24 hours, and the excess unbounded complexes were washed away thoroughly with ethanol until no red emission was detected in the washing solution under ultraviolet (UV) excitation (365 nm). Fe-HNT-Eu NC was obtained after drying at 100°C for 3 hours.

In vitro cell cytotoxicity, apoptosis, and imaging

A CCK8 assay was used to evaluate the effect of the Fe-HNT-Eu NC on the survival of LO2 and HepG2 cells, a human hepatic cell line and human hepatic adenocarcinoma cell line, respectively. LO2 and HepG2 cells were obtained from the Cell Culture Center of the Basic Institute of Medical Sciences, Peking Union Medical College (Beijing, People's Republic of China). Cells were seeded into 96-well plates in DMEM at 1×10^4 cells/well. After overnight growth, cells were cultured with the Fe-HNT-Eu NC at concentrations of 400 μg/mL, 200 μg/mL, 100 μg/mL, 50 μg/mL, 25 μg/mL, or 12.5 μg/mL for 24 hours. After 24 hours of incubation, 10 μL CCK8 was added into each well and cells were incubated at 37°C for 4 hours. Finally, the optical density was measured at 450 nm using an F50 microplate reader. At least three parallel experiments were performed.

Apoptotic rates were determined by flow cytometry using an Annexin V/PI apoptosis kit. Briefly, LO2 cells were seeded overnight at a density of 1×10^6 cells/well in six-well plates and then treated for 24 hours with Fe-HNT-Eu NC

at concentrations of 400 μg/mL, 200 μg/mL, 100 μg/mL, or 50 μg/mL. A total of 1×10^6 cells were collected by centrifugation and washed twice with cold phosphate-buffered saline. Annexin V-FITC/PI staining was performed according to the manufacturer's instructions, and the cells were analyzed using a BD Accuri C6 flow cytometer. At least three independent experiments were performed.

HepG2 cells were seeded in flat-bottomed six-well plates (Costar) in 2 mL of culture medium and incubated at 37°C with 5% CO_2. After overnight incubation, the cells were treated for 6 hours with the Fe-HNT-Eu NC at final concentrations of 50 μg/mL, and then washed three times with phosphate-buffered saline. Cell membranes were observed by fluorescence imaging using a laser scanning upconversion luminescence microscope under excitation wavelengths of 340–380 nm.

In vitro and in vivo MRI

The experimental protocol was approved by the Jiangsu University Institutional Animal Care and Use Committee and performed in accordance with the International Guiding Prinfor Biomedical Research involving Animals-1985. To evaluate the effect of Fe-HNT-Eu NC on MR enhancement, dynamic contrast-enhanced MRI was performed in vivo in tumor-bearing rabbits using the same MRI equipment as the in vitro study. Rabbits were anesthetized using isoflurane (3% loading dose, 1% maintenance dose), and Fe-HNT-Eu NC (100 mg/mL) was administered through the auricular vein at a dose of 16 mg/kg body weight. The rabbits were scanned dynamically before the experiment and also at different time points after injection (30 seconds, 3 minutes, 24 hours). The T_2-weighted sequence was as follows: repetition time (TR) =2,549 ms, echo time (TE) =100 ms, matrix =224×191, field of view (FOV) =180×180, thickness =2.0 mm, slice =12. For quantitative evaluation of the enhancement effect of the Fe-HNT-Eu NC, we obtained the T_2 signal intensity (T_2-SI) of the normal liver, muscle and liver cancer tissues using the "region of interest" function in the Philips workstation. On the traverse T_2 images, regions of interest were manually delineated on the liver and muscle tissues, and the values of the SIs were then obtained automatically.

In vivo toxicity

After the rabbits were sacrificed, their organs (heart, liver, spleen, lung, and kidney) were excised, fixed in 4% formalin, paraffin embedded, and sectioned for hematoxylin and eosin staining for histopathological analysis. The slices were observed by an Eclipse E800 microscope.

Methods of analysis and testing

Powder X-ray diffraction patterns were determined by a Rigaku-Dmax 2400 diffractometer using Cu Kα radiation over the 2θ range of 5°–70°. Transmission electron microscopy (TEM) and energy-dispersive spectrometer (EDS) were performed using a Tecnai-G2-F30 microscope at an acceleration voltage of 300 kV. Magnetization measurements were performed on a vibrating sample magnetometer (LAKESHORE-7304; VSM, Model7304, Lake shore Cryotronics Inc., Westerville, OH, USA) at room temperature. Steady-state luminescence spectra and lifetime measurements were measured on an FSL920 fluorescence spectrometer (Edinburgh Instruments Ltd) with a 450 W Xe arc lamp as the steady-state excitation source and an Nd-pumped OPOlette laser as the excitation source for lifetime measurements. For photoluminescence stability measurements, monochromatic light (360 nm) was separated from the 450 W Xe arc lamp and was used as the irradiation source with a slit of 0.2 nm and a shutter opening after 10 seconds for 800 seconds. Solutions of Fe-HNT-Eu NC at different concentrations were evaluated by T_2-weighted MRI at 3.0 T using an eight-channel phased-array coil (Achieva 3.0T TX; Philips, Amsterdam, the Netherlands). The parameters of the T_2-weighted sequence were as follows: TR =2,549 ms, TE =100 ms, matrix =224×191, FOV =120×120, thickness =2.0 mm, slice =8.

Results and discussion

Characterization of composition and microstructure

We characterized the crystal structures of unmodified HNTs, as-synthesized Fe_3O_4@HNT NC, and Fe-HNT-Eu NC using powder X-ray diffraction (Figure 2). For the

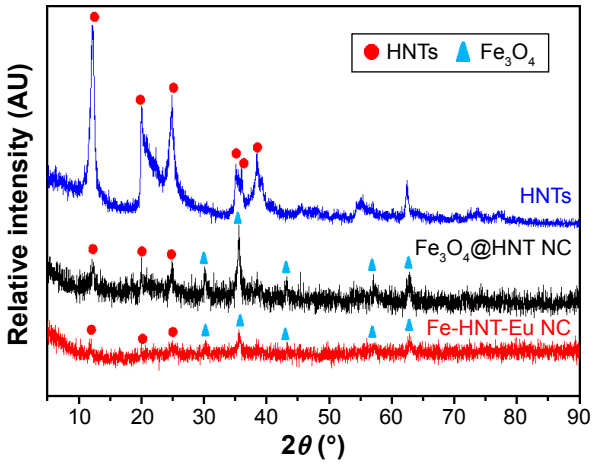

Figure 2 PXRD patterns of HNTs, Fe_3O_4@HNT NC, and Fe-HNT-Eu NC.
Abbreviations: HNT, halloysite nanotube; NC, nanocomposite; PXRD, powder X-ray diffraction.

Fe_3O_4@HNT NC, the presence of the characteristic diffraction peaks of HNTs indicates that the structure of the HNTs was maintained and that the synthetic reaction of Fe_3O_4 occurred on the surface but not in the interlayer. In addition to the characteristic diffraction peaks of HNTs, the Fe_3O_4@HNT NC exhibited additional peaks that originated from cubic Fe_3O_4, which can be assigned to the (220), (311), (400), (422), (511), and (440) planes, according to the Joint Committee on Powder Diffraction Standards (JCPDS 19-0629). After modification by PEI and the lanthanide complex, the crystal structure of the Fe-HNT-Eu NC comprised the phases of cubic Fe_3O_4 and HNTs. The diffraction peaks corresponding to the crystalline layer were greatly reduced relative to those of Fe_3O_4@HNT NC, indicating that PEI and the complex were successfully grafted onto the surface of the Fe_3O_4@HNT NC.[26]

TEM images of the HNTs and Fe-HNT-Eu NC (Figure 3A and B) confirmed that the HNTs were cylindrical-shaped tubes with an open-ended lumen along the nanotube. The TEM images also indicated that the HNTs had an external

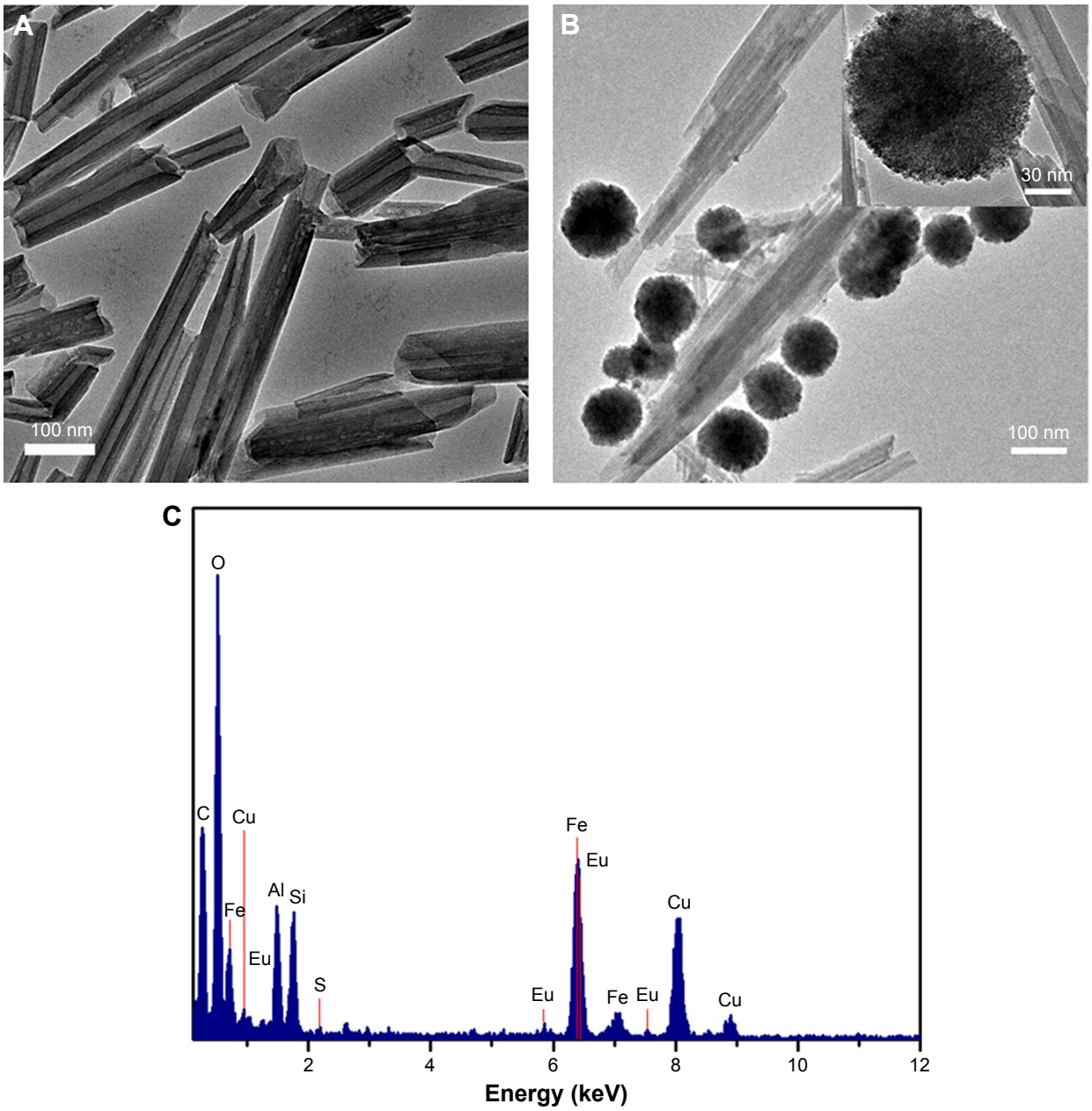

Figure 3 TEM image (**A**, **B**) and EDS spectrum (**C**) of Fe-HNT-Eu NC.
Note: The inset image is the high resolution of the Fe-HNT-Eu NC.
Abbreviations: EDS, energy-dispersive spectrometer; HNT, halloysite nanotube; NC, nanocomposite; TEM, transmission electron microscopy.

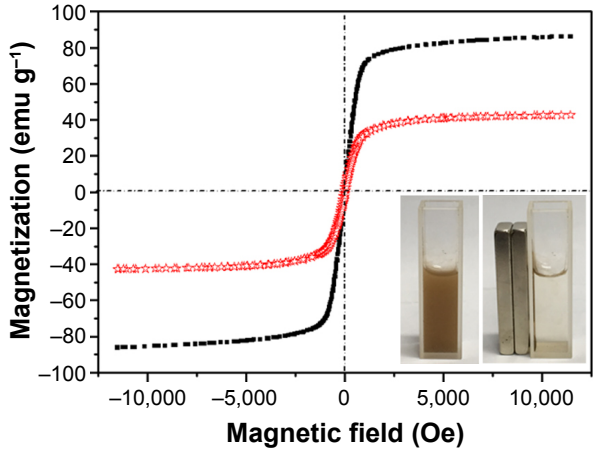

Figure 4 Magnetic hysteresis loops of pure Fe_3O_4 NP (■) and Fe-HNT-Eu NC (☆).
Note: The inset shows a photograph of Fe-HNT-Eu dispersed in water (left) and their magnetic response when placed in an external magnetic field (right).
Abbreviations: HNT, halloysite nanotube; NC, nanocomposite; NP, nanoparticle.

diameter of ~60–200 nm and an inner diameter of ~20–50 nm. Black particles (Fe_3O_4 NPs) with an average size of 100 nm were aggregated on the surface of the tube rather than in the lumen (Figure 3B). This assembly occurs because the HNTs can serve as nucleation precursors due to the high density of negative charges on their surface, which enables them to be modified by positive metal ions. In our system, iron(III) cations in solution attached to the surface of the HNTs and subsequently reduced into very fine magnetite particles in situ during hydrothermal treatment.

To confirm that Fe_3O_4@HNTs were successfully modified by Eu(III) complexes, elemental mapping analysis of Fe_3O_4@HNT and Fe-HNT-Eu NC was performed by EDS (Figure 3C). Characteristic peaks ascribed to the elements Al, Si, O, Fe, S, and Eu were observed in the EDS spectrum, indicating the successful formation of Fe-HNT-Eu NC.

The magnetic behaviors of the as-synthesized pure Fe_3O_4 NP and Fe-HNT-Eu NC were studied using a vibrating sample magnetometer at room temperature. Field-dependent magnetization curves (Figure 4) showed negligible hysteresis loops, indicating that both nanomaterials exhibited characteristic superparamagnetic behavior at room temperature. The saturation magnetization of pure Fe_3O_4 NPs was 86.02 emu g^{-1}, while that of Fe-HNT-Eu NC was 42.71 emu g^{-1} (Figure 4). The low magnetization value observed for the modified NC was due to the presence of nonmagnetic elements, such as HNTs, PEI, and Eu(III) complexes, in the conjugates. These data further reveal that the modification process does not drastically change the magnetic properties of the Fe_3O_4 NPs. The Fe-HNT-Eu NC possessed enough magnetic force to meet the needs of magnetic separation (Figure 4, inset).

Analysis of photophysical behaviors of the composites

Solid-state excitation (left) and emission (right) spectra of the Fe-HNT-Eu NC at room temperature are shown in Figure 5A. The excitation spectrum of the nanohybrids exhibits a wide wavelength range, extending from the UV region to the visible light region, with a peak at 360 nm.

In the emission spectrum, the characteristic emissions of Eu(III) arising from the transition $^5D_0 \rightarrow {}^7F_J$ (J=0, 1, 2, 3, 4) were detected under excitation at 360 nm. Red emission from the

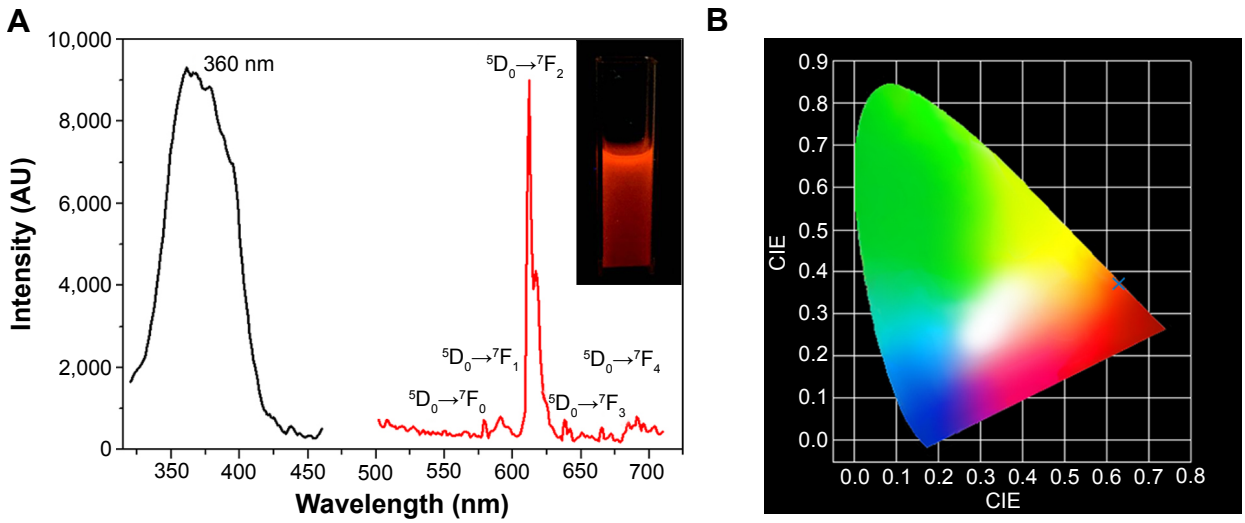

Figure 5 (**A**) Excitation and emission spectra of Fe-HNT-Eu NC, (**B**) CIE chromaticity diagram showing the (x, y) photoluminescence emission color coordinates. The inset image shows the NC dissolved in water under UVA irradiation (365 nm).
Abbreviations: HNT, halloysite nanotube; NC, nanocomposite; UVA, ultraviolet A; CIE, Commission Internationale de l'Éclairage.

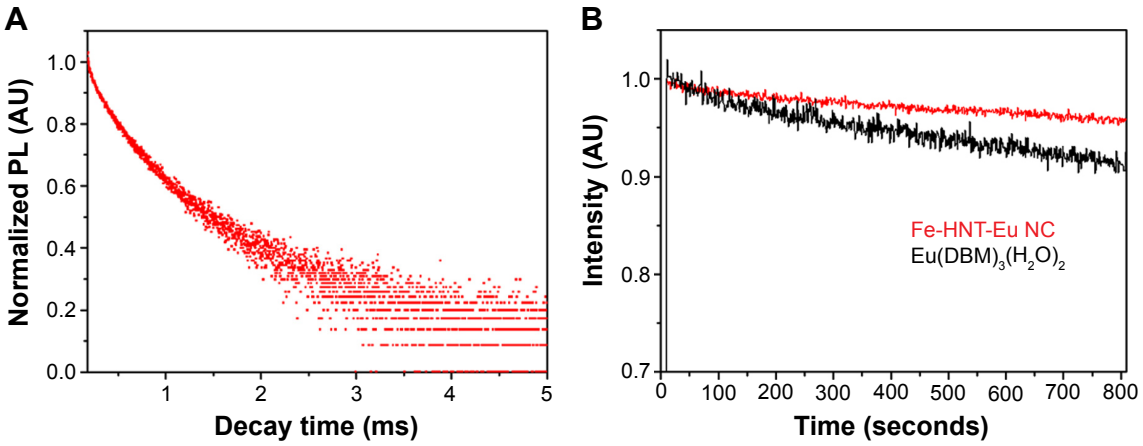

Figure 6 The emission decay curve and photoluminescence stability data.
Notes: (**A**) $^5D_0$ emission decay curve of Fe-HNT-Eu NC and (**B**) photoluminescence stability of Fe-HNT-Eu NC and the $Eu(DBM)_3(H_2O)_2$ complex.
Abbreviations: DBM, dibenzoylmethane; HNT, halloysite nanotube; NC, nanocomposite; PL, photoluminescence.

dominant transition $^5D_0 \rightarrow {}^7F_2$ at 612 nm indicates that an efficient energy transfer from the ligands to the Eu(III) metal center occurred in the nanohybrids. The Commission Internationale de l'Éclairage (CIE) chromaticity coordinates for the Fe-HNT-Eu NC were computed on the basis of the emission spectrum and were found to be (0.628, 0.371) (Figure 5B). These values are very close to the standard CIE values of the National Television System Committee for red light (x=0.670, y=0.330).

Luminescence lifetime is an important parameter for estimation of the luminescence efficiency of nanohybrids. The lifetime of the Fe-HNT-Eu NC was measured at room temperature by fitting to bi-exponential decay curves (Figure 6A). The fitting data (Table 1) show that two types of symmetrical Eu(III) sites exist in the nanohybrids. This can be attributed to site-to-site heterogeneity in the solid state.[27] The $^5D_0$ lifetime of the $Eu(DBM)_3(H_2O)_2$ complex was measured to be 53 μs;[28] the shortening of the lifetime may be due to the presence of absorbed $Eu(DBM)_3(H_2O)_2$ on the surface of the matrix. Since multi-exponential decay curves are usually observed in these types of nanohybrids,[29] the average lifetime $<\tau>$ can be calculated using the following equation:

$$<\tau>=\frac{\sum A_i \tau_i^2}{\sum A_i \tau_i} \quad (1)$$

where τ_i is the component decay time and A_i is the pre-exponential factor related to the statistical weight of each exponential. The Fe-HNT-Eu NC exhibited a longer average luminescence lifetime (310 μs) than the corresponding $Eu(DBM)_3(H_2O)_2$ complex, which indicates that the ternary europium NC was formed through the ligand exchange reaction. It also suggests that both the vibrations of the ligands around the Eu(III) metal center and the intermolecular collisions between the complexes were efficiently inhibited. The NC is expected to be suitable for use in cell imaging due to its long luminescence lifetime.

Quantum yield is another important parameter for estimation of the luminescence efficiency of the NC. We selectively determined the quantum yields (q) of the Eu^{3+}-containing NC by a previously described method (Table 1).[30] Assuming that only nonradiative (k_{nr}) and radiative (k_r) processes are involved in the depopulation of the $^5D_0$ state, q may be expressed as:

$$q=\frac{k_r}{k_r+k_{nr}} \quad (2)$$

The relationship between the radiative processes, nonradiative processes, and experimental luminescence lifetime can be estimated through the following equation:

$$k_r+k_{nr}=\frac{1}{<\tau>} \quad (3)$$

Table 1 Photoluminescence data of composites containing Eu^{3+} in solids

Parameters	Fe-HNT-Eu NC	Parameters	Fe-HNT-Eu NC
τ_1 (ms)[a]	0.505 (10.6%)	I_{00}[c]	3,692
τ_2 (ms)[a]	0.335 (89.4%)	I_{01}[c]	10,370
$<\tau>$ (ms)[a]	0.310	I_{02}[c]	72,207
ν_{00} (cm^{-1})[b]	17,271	I_{03}[c]	4,905
ν_{01} (cm^{-1})[b]	16,920	I_{04}[c]	11,583
ν_{02} (cm^{-1})[b]	16,340	k_r (ms^{-1})	0.519
ν_{03} (cm^{-1})[b]	15,674	k_{nr} (ms^{-1})	2.51
ν_{04} (cm^{-1})[b]	14,451	q (%)	17.1

Notes: [a]The lifetimes (τ) and average lifetime $<\tau>$ of the $^5D_0$ Eu^{3+} excited state obtained at room temperature. [b]Energies of the $^5D_0 \rightarrow {}^7F_J$ transitions (ν_{0J}). [c]Integrated intensities of the $^5D_0 \rightarrow {}^7F_J$ emission curves (I_{0J}).
Abbreviations: HNT, halloysite nanotube; NC, nanocomposite.

Therefore, quantum yields can be calculated from k_r and the experimental luminescence lifetime. The radiative transition rate (k_r) can be obtained by summing over the radiative rates A_{0J} for each of the $^5D_0$–^7F_J (J=0–4) transitions as follows:

$$k_r = \sum A_{0J} = A_{00} + A_{01} + A_{02} + A_{03} + A_{04} \quad (4)$$

The experimental coefficients of spontaneous emission A_{0J} can be calculated according to the following equation:[31]

$$A_{0J} = A_{01}\left(\frac{I_{0J}}{I_{01}}\right)\left(\frac{v_{01}}{v_{0J}}\right) \quad (5)$$

where A_{01} is the Einstein's coefficient of spontaneous emission between the $^5D_0$ and $^7F_1$ energy levels. Under vacuum, the value of $A_{01(vac)}$ can be taken to be 14.65 second^{-1}. When using an average index of refraction of n=1.506, the value of $A_{01}=n^3A_{01(vac)} \approx 50$ second^{-1},[32] where v_{01} and v_{0J} ($v_{0J}=1/\lambda_J$) are the energy barycenters of the $^5D_0$–$^7F_1$ and $^5D_0$–^7F_J transitions (J=0–4), respectively. The emission intensity, I, taken as the integrated intensity S of the $^5D_0$–$^7F_{0-4}$ emission curves, can be defined as follows:

$$I_{i-j} = \hbar\omega_{i-j}A_{i-j}N_i \approx S_{i-j} \quad (6)$$

where i and j are the initial ($^5D_0$) and final levels ($^7F_{0-4}$), respectively; $\hbar\omega_{i-j}$ is the transition energy; A_{i-j} is the Einstein's coefficient of spontaneous emission; and N_i is the population of the $^5D_0$-emitting level.[33] The NC exhibited relatively high luminescence quantum yield (17.1%), indicating its suitability for bio-labeling applications.

To evaluate the photoluminescence stability of the NC, we performed kinetic scans of luminescence induced by monochromic light (360 nm) partitioned from a 450 W Xe arc lamp. The dependence of the normalized emission intensity of the $^5D_0 \rightarrow {}^7F_2$ transition (612 nm) on irradiation time is shown in Figure 6B. The photoluminescence intensity of the Fe-HNT-Eu NC maintained >95% of its initial value when monitored over a period of 800 seconds under high light intensity. Compared with complex $Eu(DBM)_3(H_2O)_2$, the Fe-HNT-Eu NC showed no obvious luminescence decrease, indicating that the luminescent lanthanide ions are better protected against photobleaching when grafted onto the surface of a matrix.

Cell cytotoxicity and apoptosis

To guarantee the safety of Fe-HNT-Eu NC used as an imaging contrast agent, we assessed the effect of Fe-HNT-Eu NC on the viability of LO2 and HepG2 cells using a CCK8 assay. Untreated cells were used as controls. We observed no significant negative effect on the viability of LO2 and HepG2 cells after 24 hours of incubation with various concentrations of Fe-HNT-Eu NC (Figure 7). Cell viability remained above 81% even at a concentration of 400 μg/mL. These results indicated that Fe-HNT-Eu NCs have low cytotoxicity at the given concentration range, suggesting that they have favorable biocompatibility and the potential to be used as a medical agent.[34]

To further confirm that the NCs have no effect on the growth of human liver cells, Annexin V/PI staining and flow cytometry were used to quantify cell apoptosis.[35] Treatment with NCs at a high concentration (200 μg/mL) had no effect on the number of apoptotic LO2 cells detected by flow cytometry, indicating that the prepared NCs were suitable for biological applications (Figure 8).

In vitro cell imaging and MRI

Earlier mentioned results suggest that Fe-HNT-Eu NC is suitable for bioimaging in living HepG2 cells. We observed HepG2 cells by fluorescence microscopy and bright field imaging under normal conditions (Figure 9A–C). HepG2 cells treated with 50 μg/mL Fe-HNT-Eu NC for 6 hours exhibited an intense red fluorescence signal (Figure 9B). The overlay image (Figure 9C) of the fluorescence (Figure 9B) and bright field (Figure 9C) images indicated that the NC signal was strongly correlated with the HepG2 cells. This suggests that the obtained Fe-HNT-Eu NC is a suitable material for bioimaging and biological applications.[36] Earlier studies have reported that Fe_3O_4 can shorten T_2 relaxation time and that Fe_3O_4 NPs have great potential as MRI contrast agents.[37–39] To investigate the MRI signal enhancement effects of the

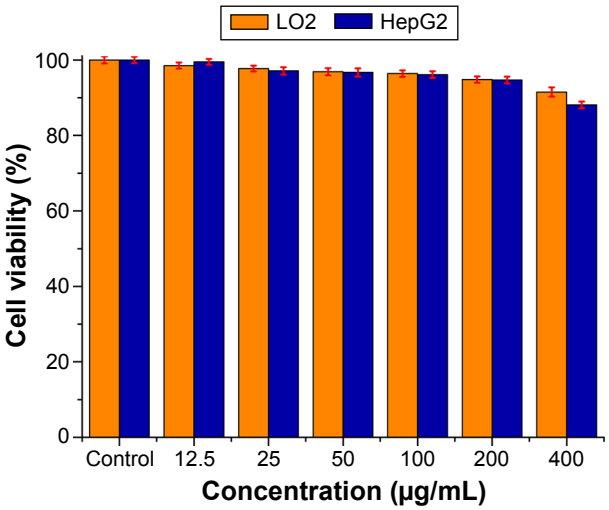

Figure 7 Viability of LO2 and HepG2 cells incubated with Fe-HNT-Eu NC at different concentrations for 24 hours.
Abbreviations: HNT, halloysite nanotube; NC, nanocomposite.

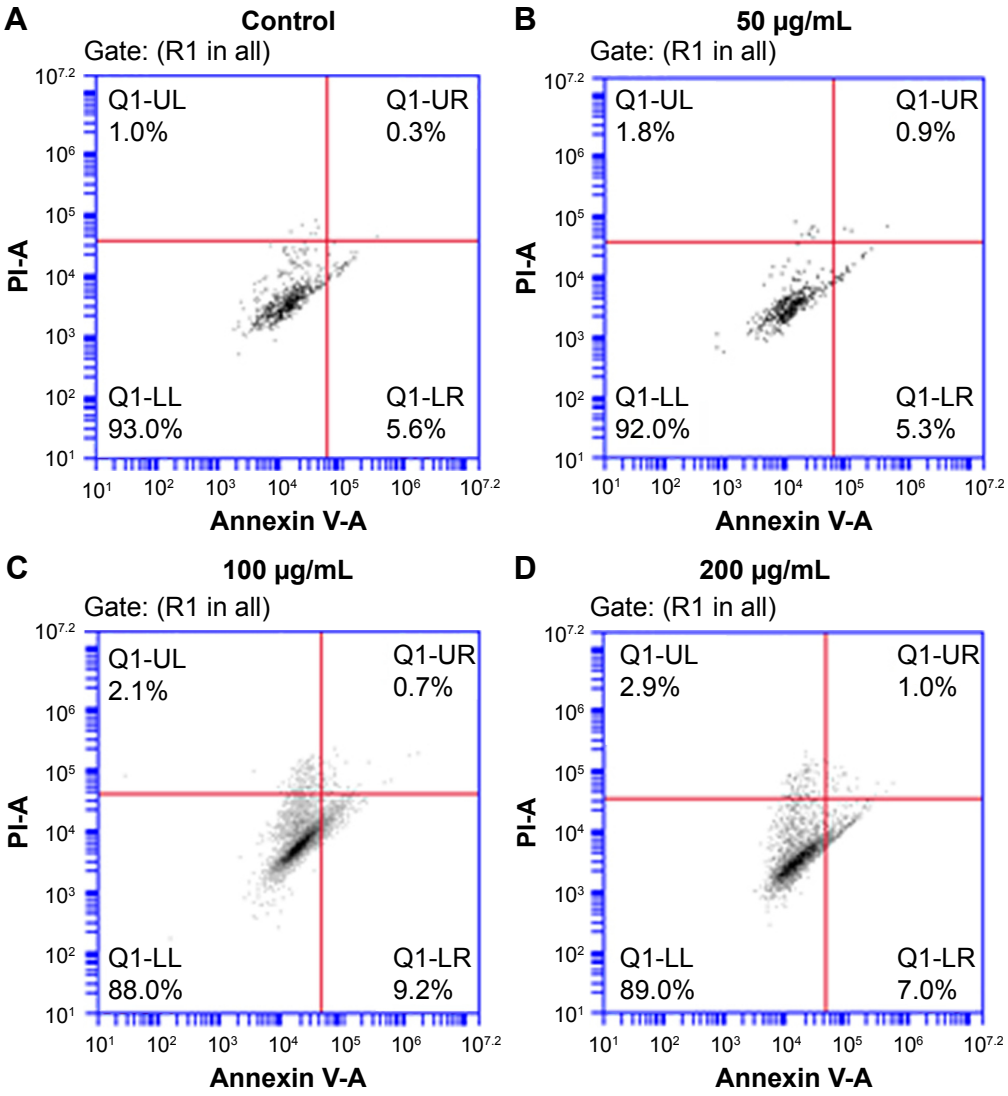

Figure 8 Annexin V/PI staining of LO2 cells incubated with Fe-HNT-Eu NC at 0 μg/mL (**A**), 50 μg/mL (**B**), 100 μg/mL (**C**), and 200 μg/mL (**D**) for 24 hours.
Abbreviations: HNT, halloysite nanotube; NC, nanocomposite; PI, propidium iodide.

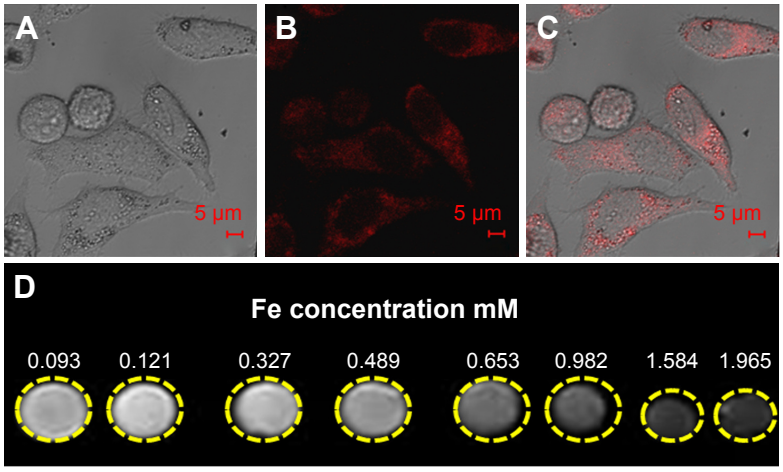

Figure 9 (**A**) Bright field image and fluorescence image; (**B**) HepG2 cells cocultured with Fe-HNT-Eu NC; (**C**) the overlapped image of images (**A**) and (**B**); (**D**) T_2-weighted MRI of Fe-HNT-Eu NC (the color change from light to dark indicates a gradual decrease in T_2-weighted MRI SI).
Abbreviations: HNT, halloysite nanotube; MRI, magnetic resonance imaging; NC, nanocomposite; SI, signal intensity.

NCs prepared in this study, the transverse relaxation time (T_2) of water protons in an aqueous solution of Fe-HNT-Eu NC was measured with a spin-echo pulse sequence. T_2-weighted images were obtained for an in vitro Fe-HNT-Eu NC solution and indicated that Fe-HNT-Eu NC can shorten the *T*2 relaxation time and lower the T_2-SI. Test tubes containing Fe-HNT-Eu NC was represented with a gray/black color in the T_2-weighted images (Figure 9D). With increasing NC concentration, the T_2-SI gradually changed from light gray to dark gray.[40] The gray value of the circles was reduced to 12.8% of its original levels by increasing the Fe concentrations from 0.093 mM to 1.965 mM, which indicated that Fe-HNT-Eu NC generated MRI contrast in T_2-weighted sequences.

In vivo MRI

To confirm the T_2 imaging capability of Fe-HNT-Eu NC, we also investigated whether it can enhance the MRI signal of normal tissues in vivo. At first, Fe-HNT-Eu NC was injected at a dose of 0.185 mmol [Fe] kg^{-1}, and then the T_2-weighted images were recorded by alternate scanning in 24 hours. Dynamic contrast-enhanced MR was performed in normal rabbit liver and muscle tissue, and four time points were aquoted before (noncontrast phase) and after the enhancement (Figure 10A–D). From the enhanced magnitudes from Figure 10E, we can see that the T_2-SI values of the normal liver, which were in the range of 30–40, were significantly decreased compared with the SIs in the noncontrast phase (decreasing value is 43). While over 3 minutes, although the T_2-SI of the liver increased, the T_2-SI was still lower than the SI in the noncontrast phase (decreasing value is 12). In contrast, the T_2-SI values of the muscle did not change significantly at any time point. This difference in signal enhancement between the normal liver and muscle tissue was due to the significantly increased blood supply of the liver, which would increase the accumulation of the intravenously injected Fe-HNT-Eu NC in hepatic region. Over the 3-minute acquisition time of the T_2-weighted image, the concentration of Fe-HNT-Eu NC in the blood vessels of the rabbit muscle was not sufficiently high to decrease the T_2-SI. Thus, we hypothesize that the Fe-HNT-Eu NC can not only enhance the T_2-weighted SI of normal liver but also indicate differences in biological characteristics (such as blood supply) between different tissues.

Furthermore, in transplanted liver cancer, the blood supply of cancerous liver is lower than that of normal liver. In addition, a fiber diolame forms around the cancerous tissue. However, the gray value of the red region in Figure 10B was still reduced to 56.6% of its original levels in Figure 10A. Earlier mentioned facts can help us to conclude that the boundary between the normal liver and transplanted cancer was more distinct in the T_2-weighted images after enhancement with Fe-HNT-Eu NC, suggesting that Fe-HNT-Eu NC can be used for tumor discovery and diagnosis.

In addition, 24 hours after the injection of the Fe-HNT-Eu NC, the T_2-SI of the normal liver was recovered to similar levels as in the noncontrast phase (Figure 10D), suggesting that the Fe-HNT-Eu NC can be metabolized effectively without leaving any residual material in the organism.

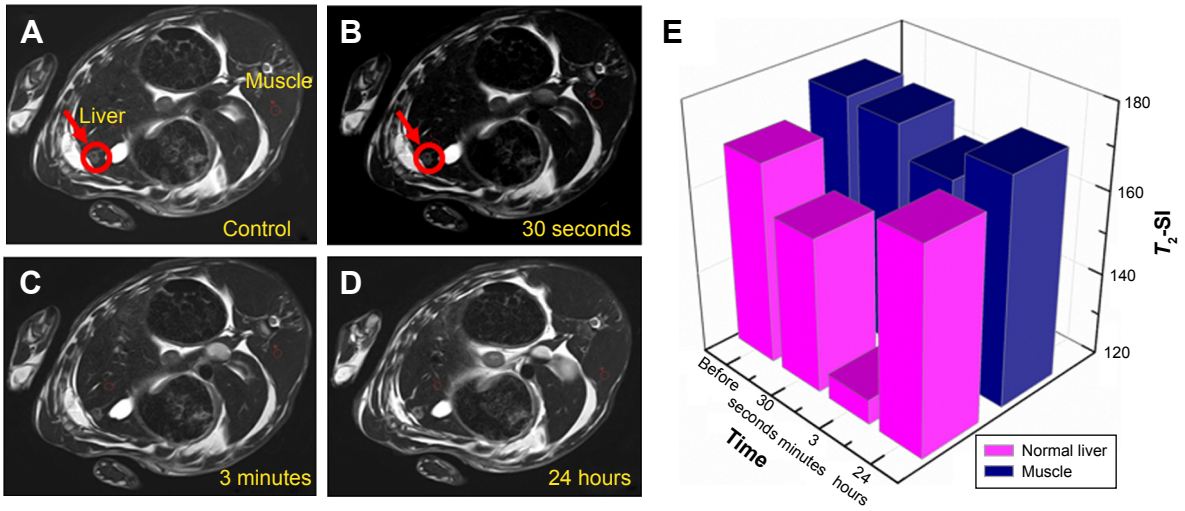

Figure 10 (**A–D**) T_2-weighted MR images of normal liver, muscle, and tissues before and after the injection of Fe-HNT-Eu NC for 30 seconds, 3 minutes, and 24 hours in rabbit. The red marker highlights the change in SI of the tumor before and after the MRI. (**E**) Mean intensity of T_2-weighted MR signals of normal liver and muscle at different times.

Abbreviations: HNT, halloysite nanotube; MR, magnetic resonance; MRI, MR imaging; NC, nanocomposite; SI, signal intensity.

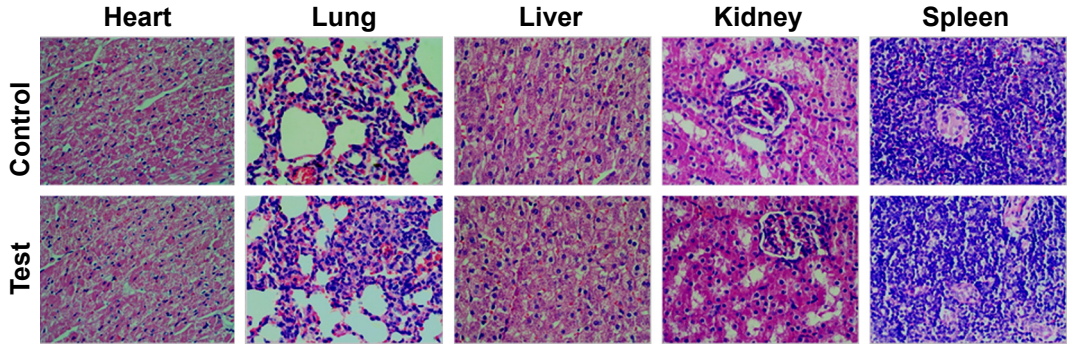

Figure 11 Histopathological analysis of rabbit heart, lung, liver, kidney, and spleen tissues after the injection with Fe-HNT-Eu NC.
Abbreviations: HNT, halloysite nanotube; NC, nanocomposite.

Overall, the current study demonstrated that Fe-HNT-Eu NCs can serve as in vitro and in vivo MRI contrast enhancers, can help distinguish between different normal tissues, and can help distinguish tumor tissues from normal tissues. These results suggest that Fe-HNT-Eu NCs have great potential as contrast agents in T_2-weighted MRI.

In vivo toxicity

We performed histopathological analysis on various tissues of rabbits to determine whether the NC caused any acute toxicity after 1-week injection of Fe-HNT-Eu NC. Analysis of tissue damage, inflammation, and lesions was performed on hematoxylin-and-eosin-stained sections of the heart, liver, spleen, lung, and kidney. Neither noticeable organ damage nor inflammation was observed in treated tissues compared with a control group (Figure 11). These results indicated that there was no significant toxicity of Fe-HNT-Eu NC at the exposure times used in this study, further demonstrating that Fe-HNT-Eu NCs have low toxicity and are safe for use in vivo.

Conclusion

A dual-modal nanoprobe Fe-HNT-Eu NC with luminescent bioimaging and T_2-weighted MRI was prepared and investigated in detail. The prepared HNT-based magnetic luminescent NC exhibited high suspension stability, low cytotoxicity, and excellent photophysical behaviors, which provided opportunities for luminescent bioimaging. The evaluation of Fe-HNT-Eu NC for contrast agent was conducted by in vitro cytotoxicity and apoptosis assay, in vitro cell imaging, in vitro and in vivo MRI, and in vivo toxicity studies in the rabbits. The results suggested that the biocompatible Fe-HNT-Eu NC prepared in this research can be used for tumor discovery and diagnosis.

Acknowledgments

This work was supported in part by the National Natural Science Foundation of China (No 21404033, No 21401046), the Technology Research Project of Henan Province (152102210314), the Foundation of the Social Development Project of Jiangsu (BE2015621), and the Natural Science Foundation of Jiangsu (BK20141122).

Disclosure

The authors report no conflicts of interest in this work.

References

1. Yan K, Li H, Wang X, et al. Self-assembled magnetic luminescent hybrid micelles containing rare earth Eu for dual-modality MR and optical imaging. *J Mater Chem B*. 2014;2(5):546–555.
2. Zhu H, Shang Y, Wang W, et al. Fluorescent magnetic Fe_3O_4/rare earth colloidal nanoparticles for dual-modality imaging. *Small*. 2013; 9(17):2991–3000.
3. Xu H, Cheng L, Wang C, Ma X, Li Y, Liu Z. Polymer encapsulated upconversion nanoparticle/iron oxide nanocomposites for multimodal imaging and magnetic targeted drug delivery. *Biomaterials*. 2011; 32(35):9364–9373.
4. Ma Q, Nakane Y, Mori Y, et al. Multilayered, core/shell nanoprobes based on magnetic ferric oxide particles and quantum dots for multimodality imaging of breast cancer tumors. *Biomaterials*. 2012;33(33): 8486–8494.
5. Park JC, Yu MK, An GI, et al. Facile preparation of a hybrid nanoprobe for triple-modality optical/PET/MR imaging. *Small*. 2010;6(24): 2863–2868.
6. Ma Y, Wang Y. Recent advances in the sensitized luminescence of organic europium complexes. *Coord Chem Rev*. 2010;254(9–10):972–990.
7. Bünzli JCG, Svetlana VE. Basics of lanthanide photophysics. In: Hänninen P, Härmä H, editors. *Lanthanide Luminescence: Photophysical, Analytical and Biological Aspects*. Berlin: Springer; 2011:1–47.
8. Zhang Y, Wei W, Das GK, Thatt T, Tan Y. Engineering lanthanide-based materials for nanomedicine. *J Photochem Photobiol C*. 2014;20(9): 71–96.
9. Comby S, Surender EM, Kotova O, Truman LK, Molloy JK, Gunnlaugsson T. Lanthanide-functionalized nanoparticles as MRI and luminescent probes for sensing and/or imaging applications. *Inorg Chem*. 2014;53(4):1867–1879.
10. Dong H, Du SR, Zheng XY, et al. Lanthanide nanoparticles: from design toward bioimaging and therapy. *Chem Rev*. 2015;115(19): 10725–10815.

11. Carlos LD, Ferreira RAS, de Zea Bermudez V, Julián-López B, Escribano P. Progress on lanthanide-based organic-inorganic hybrid phosphors. *Chem Soc Rev*. 2011;40(2):536–549.
12. Serefoglou E, Litina K. Smectite clays as solid supports for immobilization of β-glucosidase: synthesis, characterization, and biochemical properties. *Chem Mater*. 2008;20(12):4106–4115.
13. Tzialla AA, Pavlidis IV. Lipase immobilization on smectite nanoclays: characterization and application to the epoxidation of α-pinene. *Bioresour Technol*. 2010;101(6):1587–1594.
14. Vergaro V, Abdullayev E, Cingolani R, Lvov Y, Leporatti S. Halloysite clay nanotubes: characterization and biocompatibility study. *Biomacromolecules*. 2010;11(9):820–828.
15. Islam MR, Bach LG, Lim KT. Poly(2-hydroxyethyl methacrylate) grafted halloysite nanotubes as a molecular host matrix for luminescent ions prepared by surface-initiated RAFT polymerization and coordination chemistry. *Appl Surf Sci*. 2013;276(7):298–305.
16. Cavallaro G, Donato D, Lazzara G, Milioto S. Films of halloysite nanotubes sandwiched between two layers of biopolymer: from the morphology to the dielectric, thermal, transparency, and wettability properties. *J Phys Chem C*. 2011;115(42):20491–20498.
17. Jia L, Zhou T, Xu J, et al. Visible light-induced lanthanide polymer nanocomposites based on clays for bioimaging applications. *J Mater Sci*. 2016;51:1324–1332.
18. Zhou Z, Sun Y, Shen J, et al. Iron/iron oxide core/shell nanoparticles for magnetic targeting MRI and near-infrared photothermal therapy. *Biomaterials*. 2014;35(26):7470–7478.
19. Kim SM, Im GH, Lee DG, Lee JH, Lee WJ, Lee IS. Mn^{2+}-doped silica nanoparticles for hepatocyte-targeted detection of liver cancer in T-1-weighted MRI. *Biomaterials*. 2013;34(35):8941–8948.
20. Yang G, Gong H, Liu T, Sun X, Cheng L, Liu Z. Two-dimensional magnetic WS_2@Fe_3O_4 nanocomposite with mesoporous silica coating for drug delivery and imaging-guided therapy of cancer. *Biomaterials*. 2015;60:62–71.
21. He W, Cheng L, Zhang L, Liu Z, Cheng Z, Zhu X. Facile fabrication of biocompatible and tunable multifunctional nanomaterials via iron-mediated atom transfer radical polymerization with activators generated by electron transfer. *ACS Appl Mater Interfaces*. 2013;5(19):9663–9669.
22. Li MJ, Chen Z, Yam VWW, Zu Y. Multifunctional ruthenium(II) polypyridine complex-based core-shell magnetic silica nanocomposites: magnetism, luminescence, and electrochemiluminescence. *ACS Nano*. 2008;2(5s):905–912.
23. Yiu HHP, Pickard MR, Olariu CI, Williams SR, Chari DM, Rosseinsky MJ. Fe_3O_4-PEI-RITC magnetic nanoparticles with imaging and gene transfer capability: development of a tool for neural cell transplantation therapies. *Pharm Res*. 2012;29(5):1328–1343.
24. Zheng CG, Ma CL, Yu XW. Electronic effect of substituents on the DNA intercalation of ruthenium(II) polypyridyl complexes. *Chem Biodiversity*. 2011;8(8):1486–1496.
25. Melby LR, Rose NJ, Abramson E, Caris JC. Synthesis and fluorescence of some trivalent lanthanide complexes. *J Am Chem Soc*. 1964;86(23):5117–5125.
26. Zhao DF, Zhou J, Liu N. Surface characteristics and photoactivity of silver-modified palygorskite clays coated with nanosized titanium dioxide particles. *Mater Charact*. 2007;58(3):249–255.
27. Guo XM, Wang XM, Zhang HJ, et al. Preparation and luminescence properties of covalent linking of luminescent ternary europium complexes on periodic mesoporous organosilica. *Microporous Mesoporous Mater*. 2008;116(1–3):28–35.
28. Singh AK, Singh SK, Mishra H, Prakash R, Rai SB. Structural, thermal, and fluorescence properties of $Eu(DBM)_3Phen_2$ complex doped in PMMA. *J Phys Chem B*. 2010;114(41):13042–13051.
29. Wen X, Li M, Wang Y, et al. Colloidal nanoparticles of a europium complex with enhanced luminescent properties. *Langmuir*. 2008;24(13):6932–6936.
30. Werts MHV, Jukes RTF, Verhoeven JW. The emission spectrum and the radiative lifetime of Eu^{3+} in luminescent lanthanide complexes. *Phys Chem Chem Phys*. 2002;4(9):1542–1548.
31. Teotonio EES, Espínola JGP, Brito HF, et al. Influence of the N-[methylpyridyl]acetamide ligands on the photoluminescent properties of Eu(III)-perchlorate complexes. *Polyhedron*. 2002;21(18):1837–1844.
32. Hazenkamp MF, Blasse G. Rare-earth ions adsorbed onto porous glass: luminescence as a characterizing tool. *Chem Mater*. 1990;2(2):105–110.
33. Malta OL, Couto dos Santos MA, Thompson LC, Ito NK. Intensity parameters of 4f-4f transitions in the $Eu(dipivaloylmethanate)_3$ 1, 10-phenanthroline complex. *J Lumin*. 1996;69(2):77–84.
34. Xu J, Sun Z, Jia L, et al. Visible light sensitized attapulgite-based lanthanide composites: microstructure, photophysical behaviour and biological application. *Dalton Trans*. 2011;40(48):12909–12916.
35. Ma T, Xu J, Wang Y, et al. Ternary copper(II) complexes with amino acid chains and heterocyclic bases: DNA binding, cytotoxic and cell apoptosis induction properties. *J Inorg Biochem*. 2015;144:38–46.
36. Wang Y, Chang H, Jia L, et al. Development of a visible-light-sensitized THA-based lanthanide nanocomposite for cell imaging. *Mater Lett*. 2015;161:644–647.
37. Yang P, Wang F, Luo X, et al. Rational design of magnetic nanorattles as contrast agents for ultrasound/magnetic resonance dual-modality imaging. *ACS Appl Mater Interfaces*. 2014;6(15):12581–12587.
38. Yang J, Luo Y, Xu Y, et al. Conjugation of iron oxide nanoparticles with RGD-modified dendrimers for targeted tumor MR imaging. *ACS Appl Mater Interfaces*. 2015;7(9):5420–5428.
39. Wang G, Zhang X, Skallberg AS, et al. One-step synthesis of water-dispersible ultra-small Fe_3O_4 nanoparticles as contrast agents for T_1 and T_2 magnetic resonance imaging. *Nanoscale*. 2014;6(5):2953–2963.
40. Schultz-Sikma EA, Joshi HM, Ma Q, et al. Probing the chemical stability of mixed ferrites: implications for magnetic resonance contrast agent design. *Chem Mater*. 2011;23(10):2657–2664.